ELSEVIER

Journal of Fluids and Structures 26 (2010) 626–643

JOURNAL OF FLUIDS AND STRUCTURES

www.elsevier.com/locate/jfs

A CFD study of the interaction of oscillatory flows with a pair of side-by-side cylinders

Ming-Jyh Chern*, P. Rajesh Kanna[1], Yi-Jen Lu, I-Chung Cheng, Shang-Chung Chang

Department of Mechanical Engineering, National Taiwan University of Science and Technology, 43 Sec. 4 Keelung Road, Taipei 10607, Taiwan

Received 13 February 2009; accepted 26 February 2010
Available online 14 April 2010

Abstract

The behavior of vortices induced by a pair of side-by-side square cylinders in an oscillating flow is investigated using an in-house numerical model. The study is carried out for various Keulegan–Carpenter numbers, Reynolds numbers, and cylinder gap spacings. For an oscillating flow past a pair of side-by-side cylinders, the gap ratio plays a vital role in the flow pattern. A jet-like structure is observed when fluid flows through the gap. Moreover, the gap promotes the earlier appearance of asymmetric vortex shedding. In-line force and lift force coefficients of two square cylinders are analyzed using spectral analysis. An autocorrelation function is used to determine the relation between flow patterns around two cylinders. These results demonstrate the transition of the flow field from the periodic state to the chaotic state.

Keywords: Keulegan–Carpenter number; Oscillating flow; Side-by-side cylinders; Vortex dynamics

1. Introduction

Flow behind a bluff body is characterized by the fundamental flow mechanism of vortex formation. Excellent reviews on flow past a circular cylinder have been given by Zdravkovich (1997) and Williamson (1996). The interaction of an oscillating flow with a square cylinder also continues to receive considerable attention, and has practical importance, for example to the loading on a submerged structure in the near-shore region. In such cases, the oscillating flow is induced by a progressive wave train, and it is common for the submerged structure to be composed of an array of cylinders, rather than an isolated cylinder.

A past study concerned with an oscillating flow interacting with a single circular cylinder was conducted by Williamson (1985). Undertaking a series of finely controlled experiments, Williamson found that no vortex shedding occurred for Keulegan–Carpenter (KC) number less than 7. Vortex shedding commenced for KC higher than 7. A pair

*Corresponding author. Tel.: +886 2 27376496; fax: +886 2 27376460.
E-mail address: mjchern@mail.ntust.edu.tw (M.-J. Chern).
[1]Present address: Kalasalinggam University, Tamil Nadu 626 190, India.

0889-9746/$ - see front matter
doi:10.1016/j.jfluidstructs.2010.03.002

Nomenclature

B	length of a square cylinder, m
C_D	drag coefficient ($=2D/(\rho U_m^2 B)$)
C_F	in-line force coefficient ($=2D/(\rho U_m^2 B)$)
C_L	in-line force coefficient ($=2D/(\rho U_m^2 B)$)
D	drag, N
G	dimensional gap between two square cylinders, m
g^*	nondimensional gap between two square cylinders ($= G/B$)
KC	Keulegan–Carpenter number ($= U_m T_0/B$)
L	lift, N
P	nondimensional pressure
Re	Reynolds number ($= U_m B/v$)
St	Strouhal number
T	nondimensional time
T^*	period of an oscillating flow, s
t	time, s
U_m	amplitude of velocity variation, m s^{-1}
U	nondimensional velocity vector
u	velocity component in the x-direction, m s^{-1}
v	velocity component in the y-direction, m s^{-1}
Greek symbols	
v	kinematic viscosity of working fluids, m s^{-2}
ω	angular frequency, s^{-1}
Superscripts	
D	downstream cylinder
U	upstream cylinder
Subscripts	
i	initial time
f	final time

of symmetric vortices was shed from a circular cylinder for $7<\mathrm{KC}<15$. The number of pairs of detached vortices was proportional to the KC number. Above a critical value of KC, the vortex shedding became asymmetric. Subsequently, Williamson (1985) studied cases involving a pair of circular cylinders and various other arrangements. Time histories of drag and lift coefficient were obtained, and the anti-phase and in-phase modes of vortex shedding observed. Obasaju et al. (1988) focused on the relationship between KC number and the number of vortices shed. They found the number of vortices shed remained the same until a certain threshold value of KC was reached, above which the number of vortices shed continued to increase. Sumer and Fredsoe (1997) summarized Williamson's (1985) and Sarpkaya's (1986) results and classified flow patterns according to the behavior of vortex shedding. The first phase comprised no separation in creeping flow for $\mathrm{KC}<1.1$. The second phase involved separation resulting in Honji (1981) vortices for $1.1<\mathrm{KC}<1.6$. The third phase was characterized by a pair of vortices for $1.6<\mathrm{KC}<4$.

Yang et al. (2005) reported numerical simulations of flow past an oscillating rectangular cylinder in a channel, and found that the vortex shedding frequency gradually changed to match the cylinder oscillating frequency. Testik et al. (2005) studied the steady and oscillating flow of a single horizontal bottom cylinder, and reported that the near wake was dominated by large vortices of sizes comparable to the size of the cylinder. Zhou et al. (2000) obtained experimental results for two and three parallel circular cylinders, focusing on momentum, as well as heat transfer, in the wake region. They found that the heat flux gradient did not approach zero near the centerlines of simple wakes, which caused a significant drop in the turbulent Prandtl number.

Bearman et al. (1984) used flow visualization experiments to observe the oscillating flow past a square cylinder. They investigated the effect of incident angle of the oscillating flow and the effect of rounding the corners of the cylinder on the resultant force exerted on the cylinder. They found that round corners affected the drag coefficient of the square cylinder in an oscillating flow more noticeably than in a uniform flow. Zheng and Dalton (1999) employed a numerical model based on a finite difference method to simulate an oscillating flow interacting with a square cylinder and a diamond cylinder within the following ranges: $200<\mathrm{Re}<1000$ and $1<\mathrm{KC}<5$. They determined lift and in-line force coefficients, and identified irregular waveforms in time histories of the in-line force coefficients, which appeared when vortex shedding became asymmetric and chaotic due to nonlinear flow dynamics. They also discussed the effect of round corners on the force coefficients, and noted that these corners have a significant effect on an oscillating flow. Chern et al. (2007) performed numerical simulations to observe the interaction of oscillatory flow with a single square cylinder at moderate Reynolds and KC numbers. Spectral analysis of the in-line force coefficients was utilized to show the route of the flow system from order to chaos. Recently, Peng (2004) studied vortex shedding behind a pair of square cylinders immersed in uniform upstream flow using flow visualization and numerical simulation. He observed in-phase and anti-phase vortex shedding modes depending on Reynolds number and gap ratio between the cylinders. He found that the in-phase vortex shedding was not spatially stable, unlike anti-phase vortex shedding.

The present study examines the interaction of an oscillating fluid flow with a pair of side-by-side square cylinders. An established numerical model is utilized to simulate the flow features in the vicinity of the two cylinders, and determine the time histories of the in-line and lift coefficients. Phase diagrams of lift and in-line force coefficients are presented that demonstrate the route of vortex systems around cylinders from order to chaos.

2. Mathematical formulae and numerical model

We consider the oscillating flow of an incompressible fluid in two dimensions. As indicated in Fig. 1, two square cylinders, each of size B, are located at the middle of the domain with gap G between them. The oscillating flow condition is imposed at the four open boundaries as

$$u = U_m \sin(\omega t), \tag{1}$$

where u is the time-dependent flow velocity (in the x-direction), U_m the magnitude of the imposed oscillatory flow velocity, ω the angular frequency of the oscillating flow, and t is time. No-slip boundary conditions are imposed at the solid boundaries of cylinders. The continuity (mass conservation) equation and Navier–Stokes (momentum conservation) equations are

$$\nabla \cdot \mathbf{U} = 0, \tag{2}$$

and

$$\frac{\partial \mathbf{U}}{\partial t} + \nabla \cdot (\mathbf{U}\mathbf{U}) = -\nabla P + \frac{1}{\mathrm{Re}} \nabla^2 \mathbf{U}, \tag{3}$$

where $\mathbf{U}$ and P are nondimensional velocity and pressure, respectively. The amplitude of incident velocity U_m and the length B of the side of the square cylinder are used as the characteristic velocity and length, respectively. Re is the Reynolds number given by $U_m B/\nu$, where ν is the kinematic viscosity of the fluid.

The finite volume method is employed to discretize Eqs. (2) and (3). The 4th-order Adams–Bashforth scheme is used for the temporal derivative. The third-order QUICK scheme proposed by Leonard (1979) is employed for the advective derivative. To solve the pressure field, the SOLA algorithm is implemented. Although Zheng and Dalton (1999) have discussed the treatment of sharp corners, where the solution is discontinuous due to a singularity, no special treatment has been given in more recent studies (Yang et al., 2005; Peng, 2004; Bhattacharyya and Maiti, 2004) of flow past sharp corners. In the more recent studies, staggered grids were adopted to eliminate computational nodes at corner points. Hence, a staggered grid arrangement is used to simulate the solution domain in the present study. There is no node to determine velocity or pressure at corner points.

Zheng and Dalton (1999) have studied the effect of the computational domain and grid independence for the oscillating flow interacting with a square cylinder. They utilized a $20B \times 20B$ square domain for their numerical model, and employed various uniform meshes, including 65×65, 129×129, and 257×257 to verify the grid independence of their model. The pressure coefficient was determined using various meshes. Consequently, results given by the meshes 129×129 and 257×257 were very close. In the present study, 105×105, 211×211, and 251×251 uniform meshes were utilized to investigate the influence of the grid in cases with a single square cylinder. As can be seen from Table 1, the time-averaged in-line force coefficients, C_F, given by 211×211 and 251×251 are very similar. Following Zheng and Dalton (1999) and also noting the results in Table 1, the 251×251 mesh was therefore adopted in the present study. Furthermore, we used $21B \times 21B$, $21B \times 25\ B$, $25B \times 25B$, and $30B \times 30B$ meshes to explore their effects for an

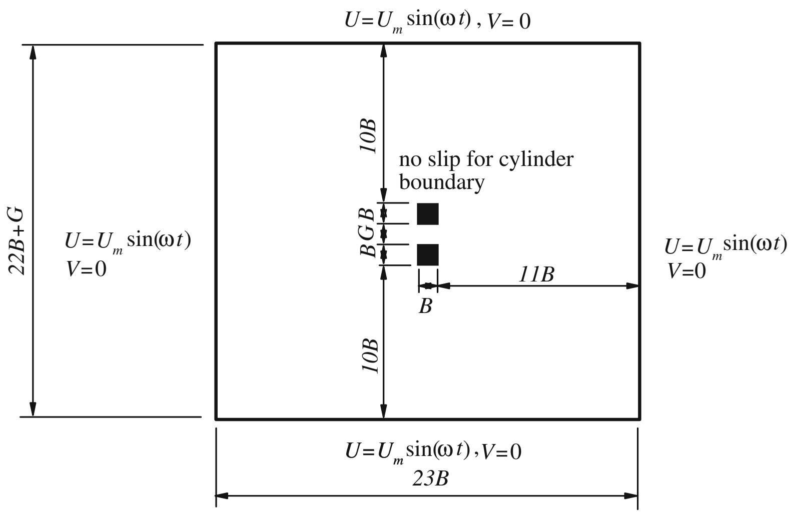

Fig. 1. Schematic diagram of the oscillating flow and square cylinders.

oscillating flow interacting with a single square cylinder. The predicted time-averaged in-line force coefficients C_F given by these meshes were very close. Thus, $23B(22B+G)$ is adopted as the computational domain in which there is no vortex shedding in the flow field, where G is the gap between cylinders. For cases with vortex shedding, the $23B(45B+G)$

Table 1
Comparison of time-averaged in-line force coefficient C_F, for an oscillating flow interacting with a single cylinder. Re = 213 and KC = 1.

Mesh size	Present study	Zheng and Dalton (1999) (numerical result)	Bearman et al. (1984) (experimental result)
105×105	38.685	33.128	27.409
211×211	33.343		
251×251	33.398		

Table 2
Comparisons of obtained time-averaged C_D, amplitude of C_L, and St with available studies for a uniform flow past a square cylinder.

	Re = 100			Re = 200		
	C_D	C_L	St	C_D	C_L	St
Present study	1.61	±0.42	0.13	1.62	±0.60	0.145
Okajima et al.	N/A	±0.5	0.141	N/A	±1.3	0.142
Davis et al.	1.66	±0.36	0.164	1.79	±0.38	0.179
Franke et al.	1.61	±0.27	0.154	1.60	±0.62	0.157
Saha et al.	1.51	N/A	0.159	1.67	N/A	0.163

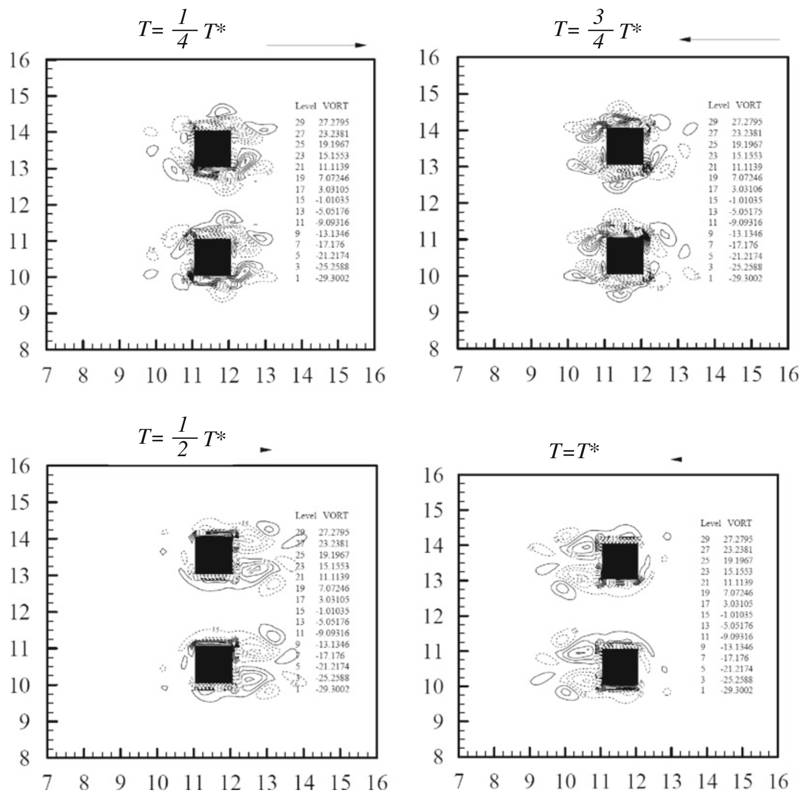

Fig. 2. Vorticity contours at the 10th period; $g^* = 2$, Re = 300, and KC = 5.

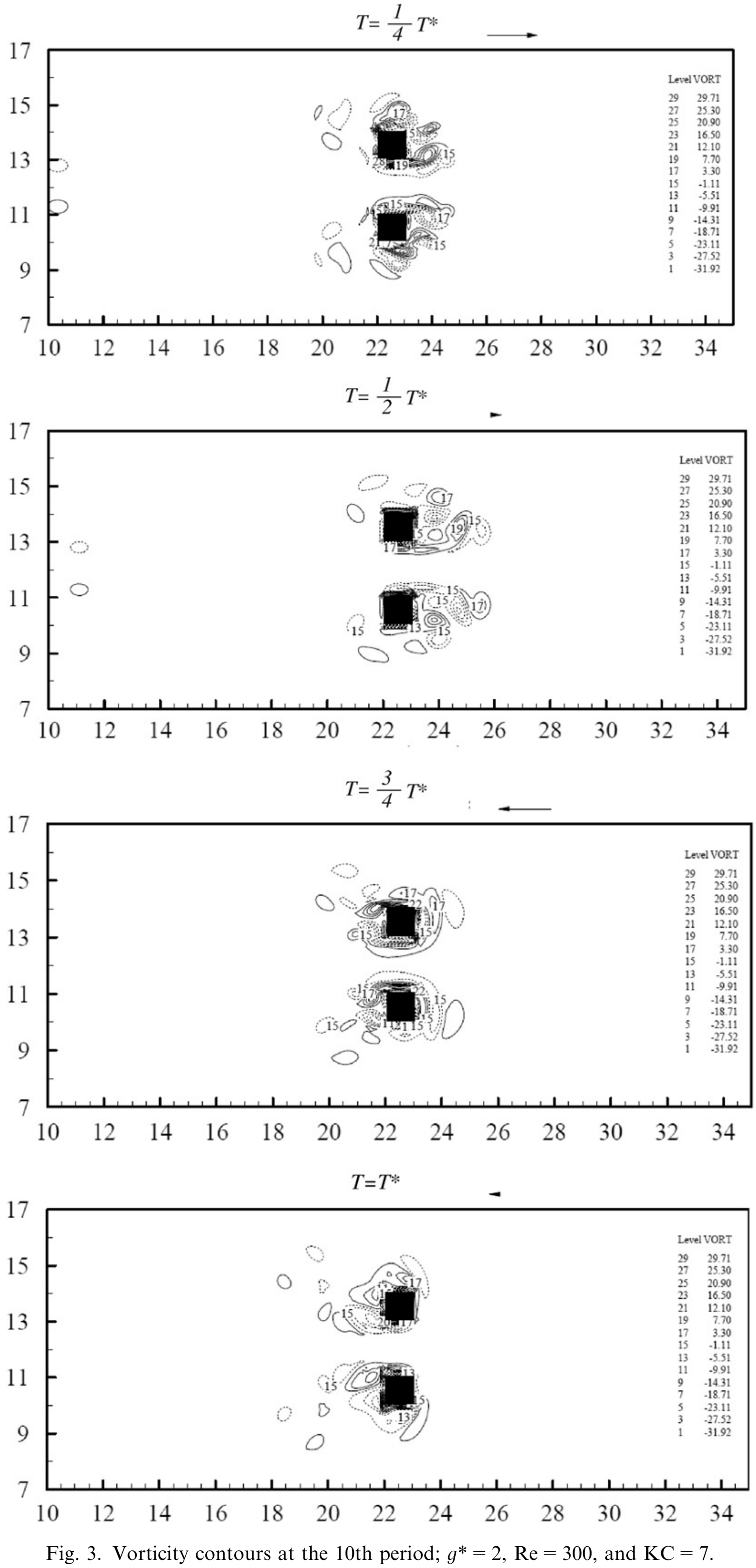

Fig. 3. Vorticity contours at the 10th period; $g^* = 2$, Re = 300, and KC = 7.

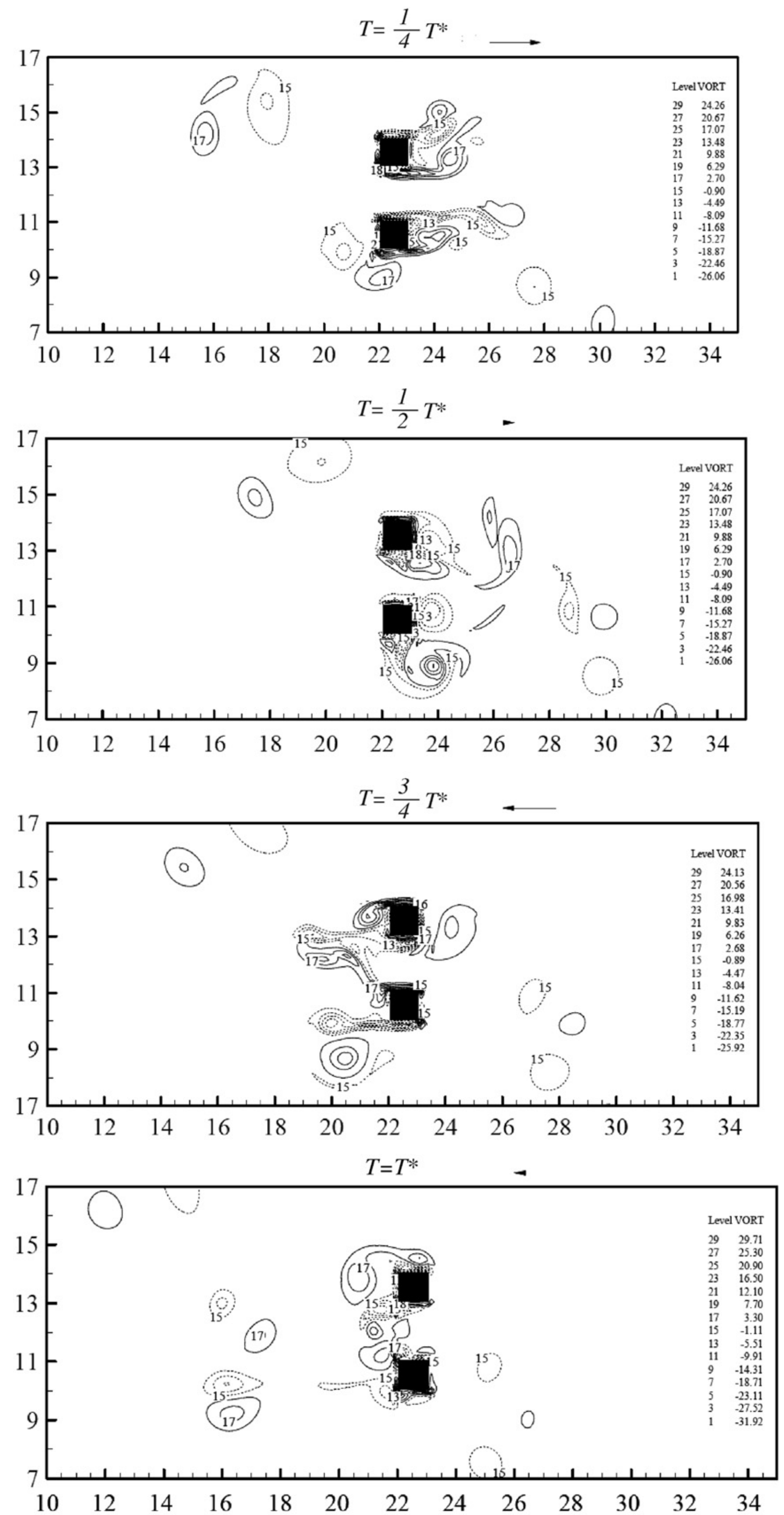

Fig. 4. Vorticity contours at the 10th period; $g^* = 2$, Re = 300, and KC = 15.

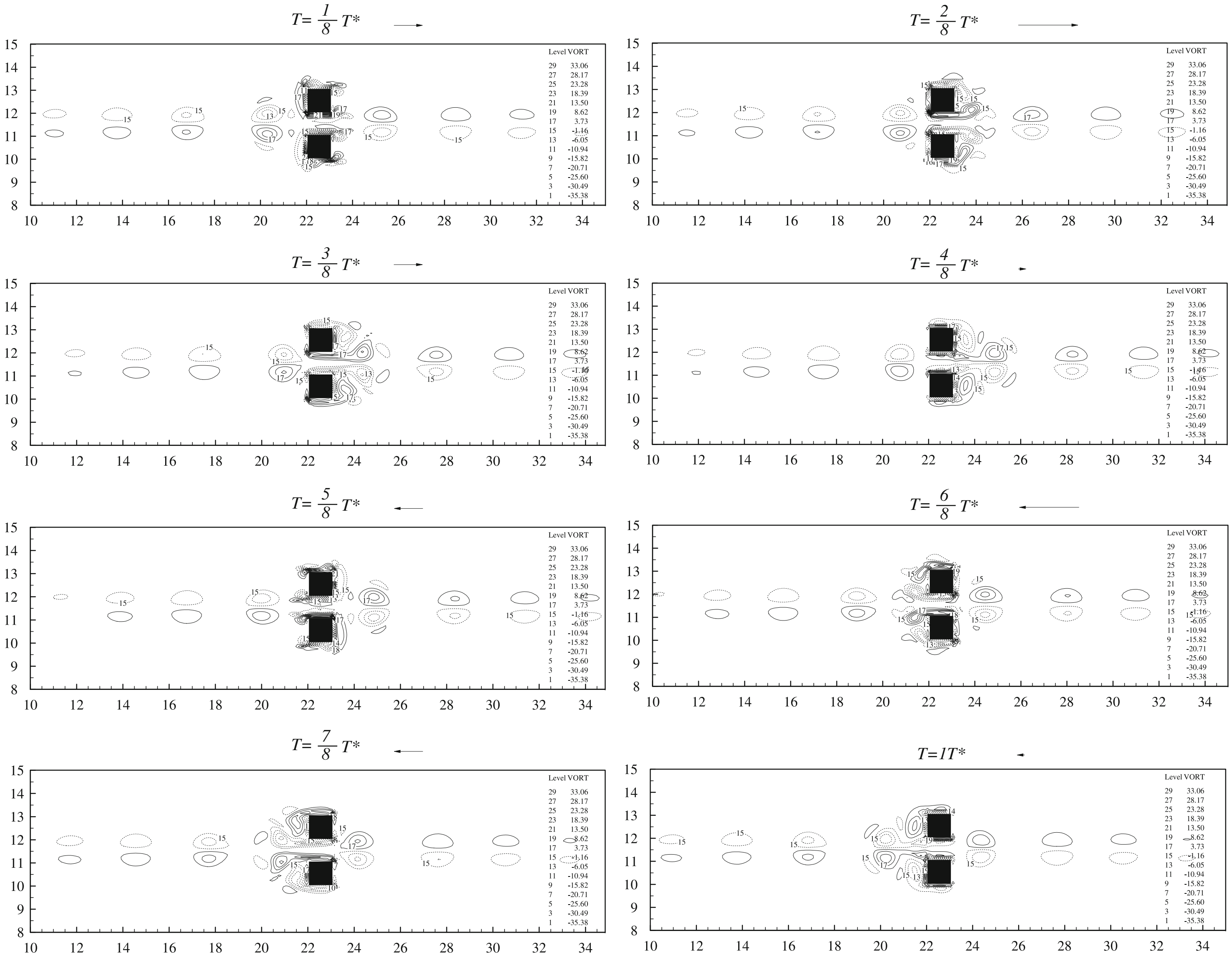

Fig. 5. Vorticity contours at the 10th period; $g^* = 1$, Re = 300, and KC = 7.

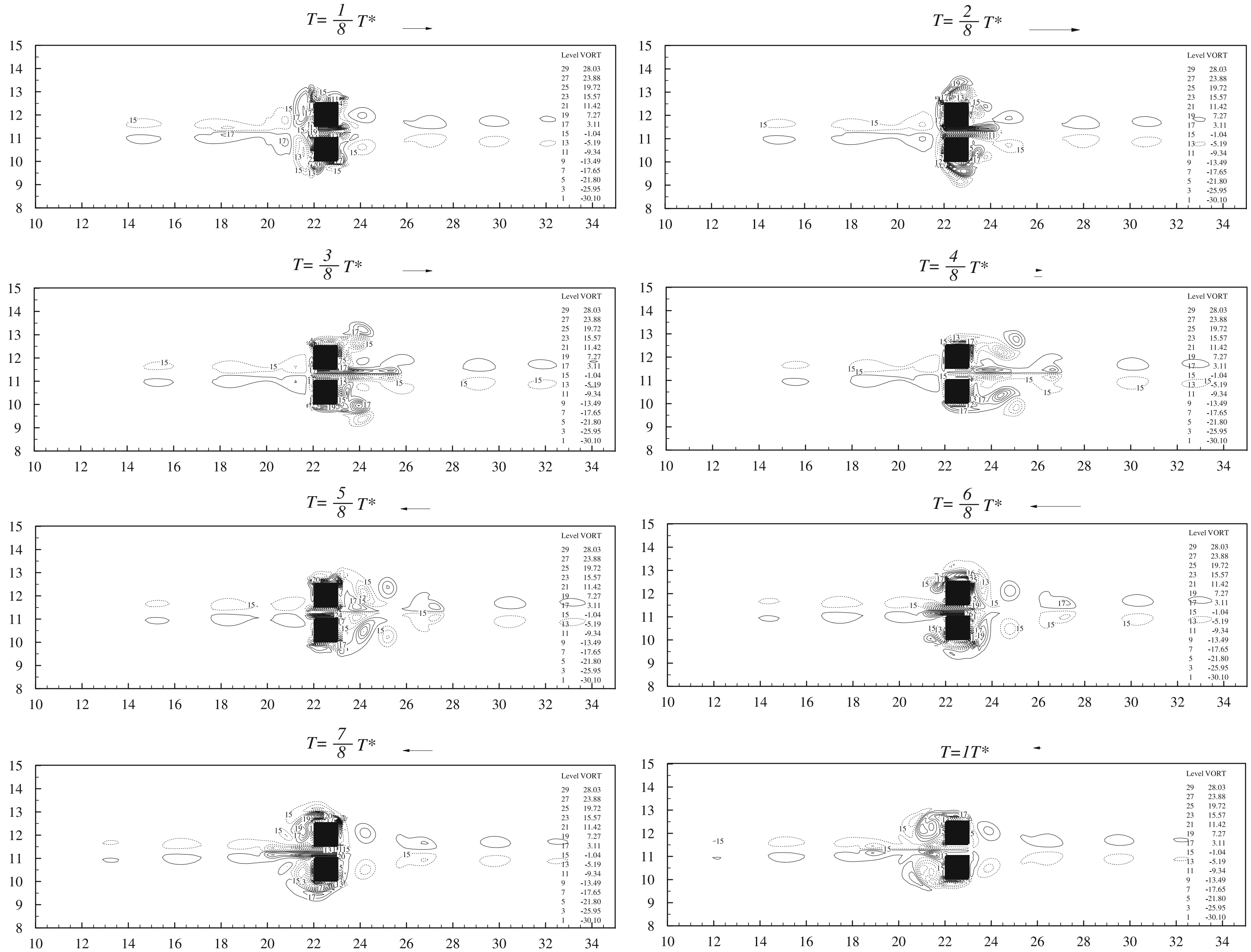

Fig. 6. Vorticity contours at the 10th period; $g^* = 0.5$, Re = 300, and KC = 7.

computational domain was used to ensure that no vortex passes through any boundary. The present results are in good agreement with those of Zheng and Dalton (1999); the difference in time-averaged C_F (see Table 1) is only 0.8%.

The numerical model was executed on a Linux-based cluster containing eight nodes, based on Advanced Micro Devices (AMD) central process units.

2.1. Validation of proposed numerical model

The numerical model was validated for uniform flow past a square cylinder. This benchmark case has been studied by Okajima et al. (1992), Davis et al. (1984), Franke et al. (1990), and Saha et al. (2000). Relevant physical coefficients, including the time-averaged drag coefficient (C_D), the amplitude of lift coefficient (C_L), and Strouhal number (St), were used to verify the proposed model. Two flow fields at Reynolds numbers (Re) 100 and 200 were simulated. The results listed in Table 2 show that acceptable agreement has been obtained between the present study and previous simulations.

The second validation test comprised the interaction of an oscillating flow with a single square cylinder using various meshes at Re = 213 and KC = 1. Table 1 lists the resultant time-averaged in-line force coefficient C_F obtained using the present model and by Zheng and Dalton (1999) and Bearman et al. (1984). It is found that the time-averaged C_F given by the established model is independent of meshes denser than 211×211. Moreover, the present result is within 1% of that of Zheng and Dalton (1999). However, the present result was 21% different from that reported by Bearman et al. (1984).

Taken overall, the validation results indicate that the present model is suitable for investigating an oscillating flow interacting with a pair of square cylinders.

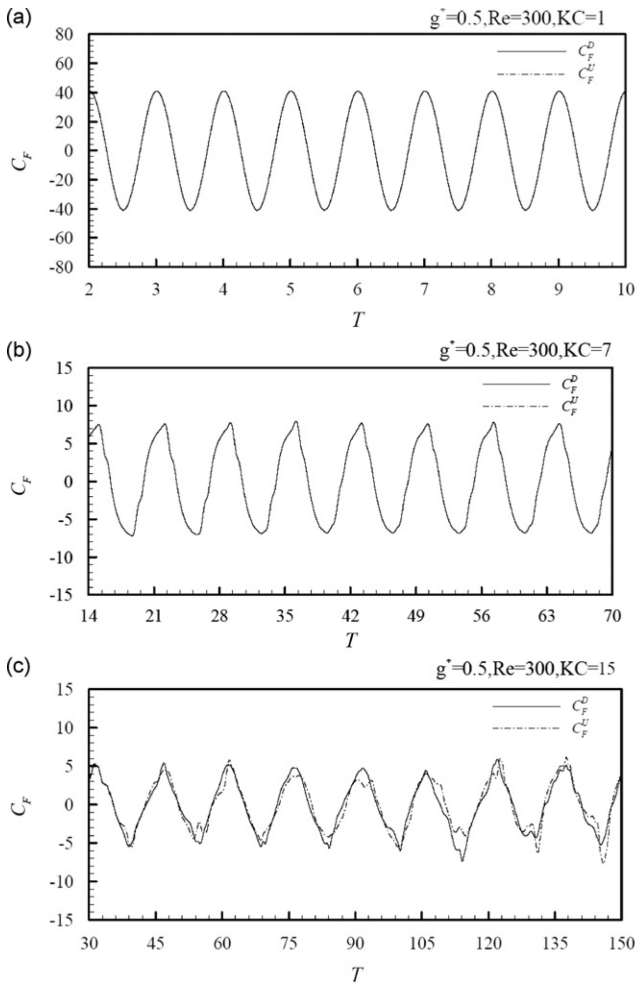

Fig. 7. Time histories of C_F at $g^* = 0.5$, Re = 300, KC = 1, 7, and 15.

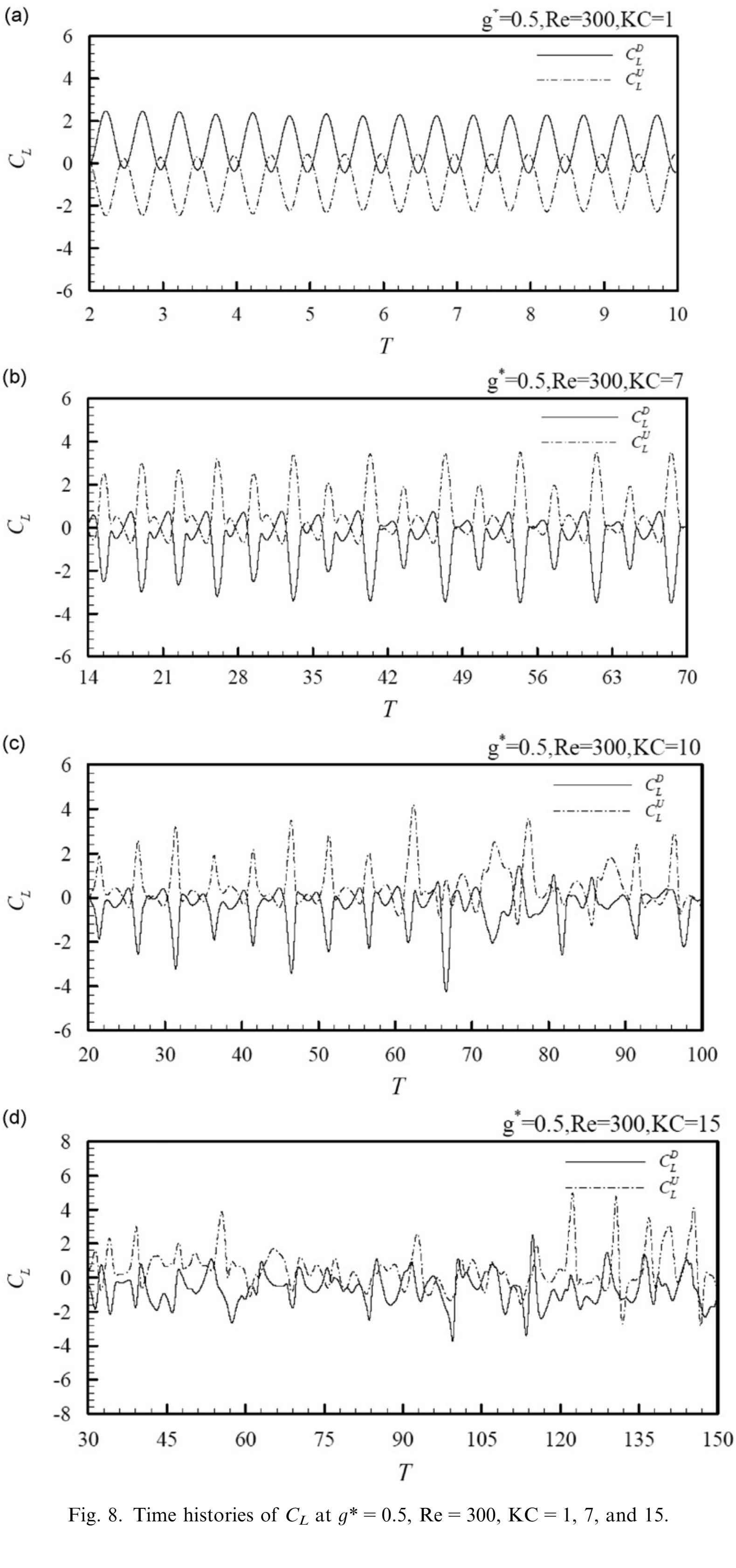

Fig. 8. Time histories of C_L at $g^* = 0.5$, Re = 300, KC = 1, 7, and 15.

3. Results and discussion

The three main nondimensional parameters are the Reynolds number (Re), Keulegan–Carpenter number (KC), and the dimensionless gap (g^*) between the two cylinders. Here, we define the Keulegan–Carpenter number as

$$\mathrm{KC} = \frac{U_m T^*}{B}, \tag{4}$$

where T^* is the period of an oscillating fluid flow. The ranges of Re, KC, and g^* considered in the present study are 200–500, 1–15, and 0.5–2.0, respectively.

3.1. Flow patterns

Flow variations of an oscillatory flow interacting with a single square cylinder have been reported by Zheng and Dalton (1999) and Chern et al. (2007). Vortex systems adjacent to two square cylinders are independent, provided the gap between the cylinders is large. In other words, each vortex system adjacent to a cylinder behaves independently, like that of an oscillatory flow interacting with a single cylinder. However, when the gap is reduced, the vortex systems will begin to interact with each other. The present work will determine the influence of the gap on those vortex systems, by examining the effect of different gap spacings.

First, consider the results for a dimensionless gap, $g^* = 2$. No vortex appears when KC is less than 3. A pair of symmetric vortices appears when KC is larger than 3. Fig. 2 shows the behavior of symmetric vortex pairs at KC = 5. The pairs develop at the lower sides of cylinders for a half period. They form first at the first quarter period and subsequently fade. When the flow changes direction at the other half period, two new pairs of symmetric vortices are found at the other side of the cylinders. Meanwhile, the vortices do not shed from the cylinders even at the 10th period. Pairs of symmetric vortices can be found when KC < 7 (see Fig. 3). As KC is increased, the symmetry in the vortex pairs cannot be retained. As a result, the vortex pairs are asymmetric but are attached to the cylinders. For KC > 10,

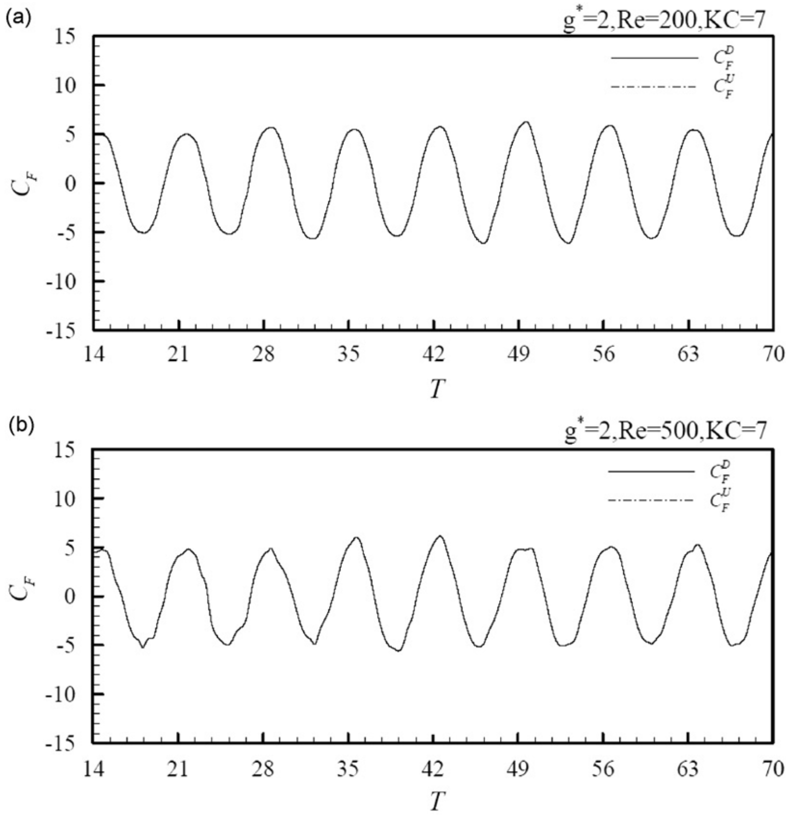

Fig. 9. Time histories of C_F at $g^* = 2$, Re = 200 and 500, KC = 7.

asymmetric vortex shedding occurs from both cylinders. When these asymmetric vortices are shed from the cylinders, they interact with other residual vortices. Fig. 4 shows asymmetric vortex shedding from the cylinders for KC = 15.

Second, consider flows with $g^* = 1$. When the gap between two square cylinders is reduced, the flow field changes and the gap flow has a significant effect on the vortices. For KC < 3, vortices do not develop. For KC > 3, a pair of symmetric vortices grows adjacent to the cylinders. Fig. 5 shows the vorticity contours at KC = 7. Due to the interaction between vortices of opposite sign at the small gap, the vortices adjacent to the gap are stretched toward the flow direction as shown at $T = \frac{3}{8}T^*$ and $\frac{4}{8}T^*$. The effect is the same as in Fig. 3. When the flow changes direction, vortices beyond the gap are dissipated. However, vortices adjacent to the gap are not dissipated completely at $T = \frac{5}{8}T^*$. This is different from the previous case for $g^* = 2$. The vortices do not vanish. When the flow changes direction again, the vortices are pushed downstream by the gap flow. After several cycles, the vortices migrate further from the cylinders and become damped. In general, when g^* is 1, the vortex pair behind each square cylinder is different from that of a single cylinder.

Third, consider flows with $g^* = 0.5$. No vortex is observed in the flow field at KC < 3. As KC increases to 7, a pair of asymmetric vortices is generated in the vicinity of the pair of square cylinders. Fig. 6 shows the situation at the 10th period when KC is 7. Due to the strong gap flow, the vortices near the gap appear when the oscillatory flow is decelerated at $T = \frac{4}{8}T^*$. Subsequently, the vortices near the gap are expelled. These two vortices become weak while traveling far away from the cylinders in later cycles. Two vortices away from the gap are created that then disappear as the oscillatory flow is accelerated and decelerated at $T = \frac{1}{8} - \frac{4}{8}T^*$. The temporal and spatial variations of these two vortices are similar to those in the vicinity of a single cylinder, due to the narrow gap. These vortices are not adjacent to the cylinders when KC increases.

3.2. Variation of the resultant force

Time histories of force coefficients are calculated in order to estimate the influence of the oscillating fluid flow on the square cylinders. The resultant force exerted on the square cylinder is determined by the numerically predicted pressure and shear stress distributions. The components of the resultant force parallel to and normal to the flow direction are

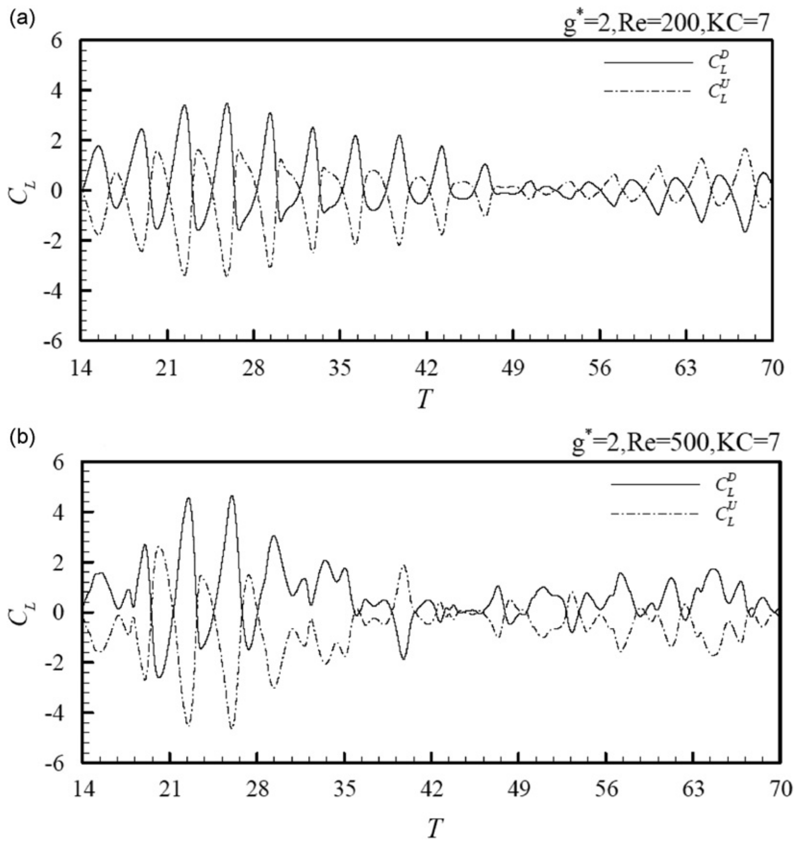

Fig. 10. Time histories of C_L at $g^* = 2$, Re = 200 and 500, KC = 7.

called the in-line force D and lift force L, respectively. In order to analyze the interaction of vortices quantitatively, the forces exerted on the square cylinders are computed. Fig. 7(a)–(c) presents time histories of in-line force coefficients C_F at $g^* = 0.5$ for the upstream cylinder, C_F^U and the downstream cylinder, C_F^D. When KC < 5 (see Fig. 7(a)), variations of C_F of two cylinders behave sinusoidally and are almost the same. Moreover, the waveforms are very close and small undulations form at KC = 7 (Fig. 7(b)). These results show that nonlinearity grows in the resultant forces. Subsequently, the irregularity becomes more obvious at KC > 10 (see Fig. 7(c)). Meanwhile, the waveforms gradually separate from each other, due to the formation of asymmetric vortices at higher KC values. Furthermore, KC increases when C_F is reduced significantly.

Fig. 8(a)–(d) shows the lift coefficient (C_L) for $g^* = 0.5$ for various KC values. When KC is 1, C_L becomes sinusoidal (Fig. 8(a)), and the upstream and downstream cylinder vortices result in an anti-phase mode. The period as well as magnitude is reduced when KC is increased. C_L is periodic up to KC = 7. However when KC is increased to 10 and when time elapses beyond $T = 68$, an irregularity is found (Fig. 8(c)). This irregularity begins at an earlier stage when KC is further increased (Fig. 8(d)). The magnitude of C_L^U is negative at low KC values and becomes positive when KC is increased. The behavior reverses for C_L^D. Time histories of in-line force and lift coefficients for Re = 200 and 500 are shown in Figs. 9 and 10, respectively, for $g^* = 2$ and KC = 7. The value of C_F is periodic for Re = 200. There is no variation in C_F between the upstream cylinder (C_F^U) and downstream cylinder (C_F^D) for different Re values. However, the signs of the magnitudes of C_L are opposite for different Re in Fig. 10.

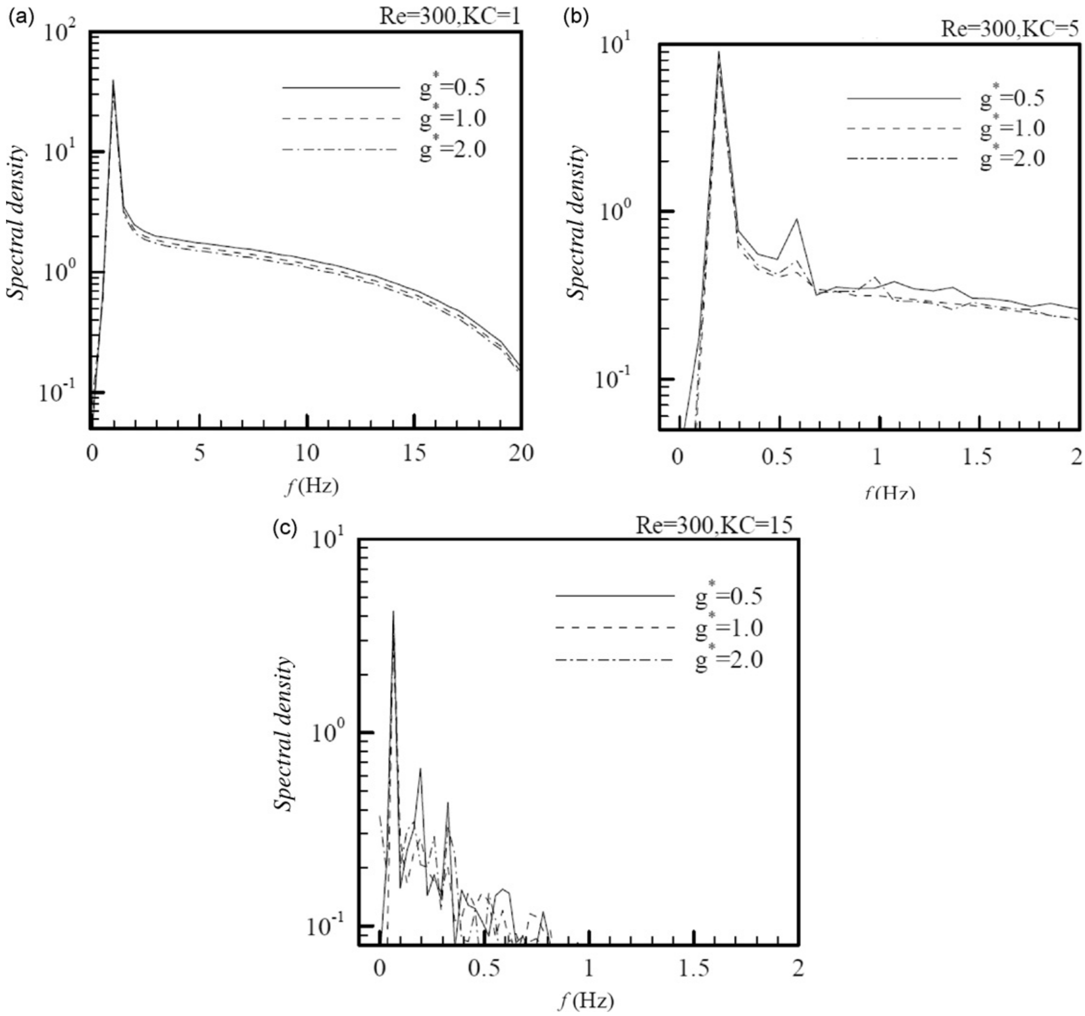

Fig. 11. Power spectrums of C_F for Re = 300, $g^* = 0.5$, 1, and 2, and KC = 1, 5, and 15.

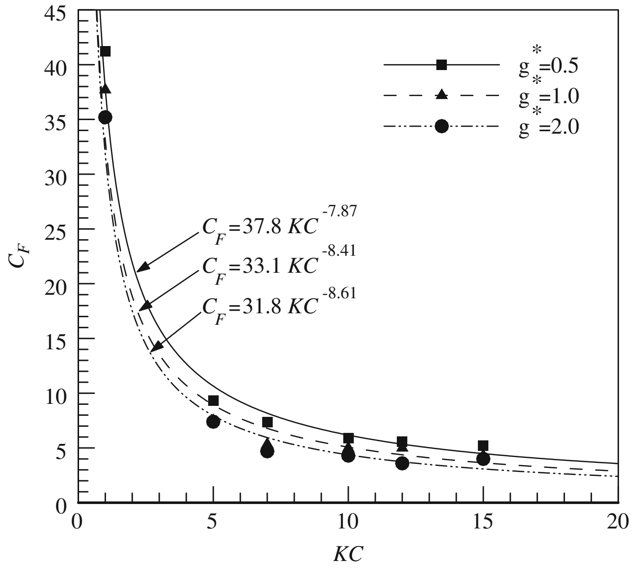

Fig. 12. Variation of time-averaged C_F with respect to KC.

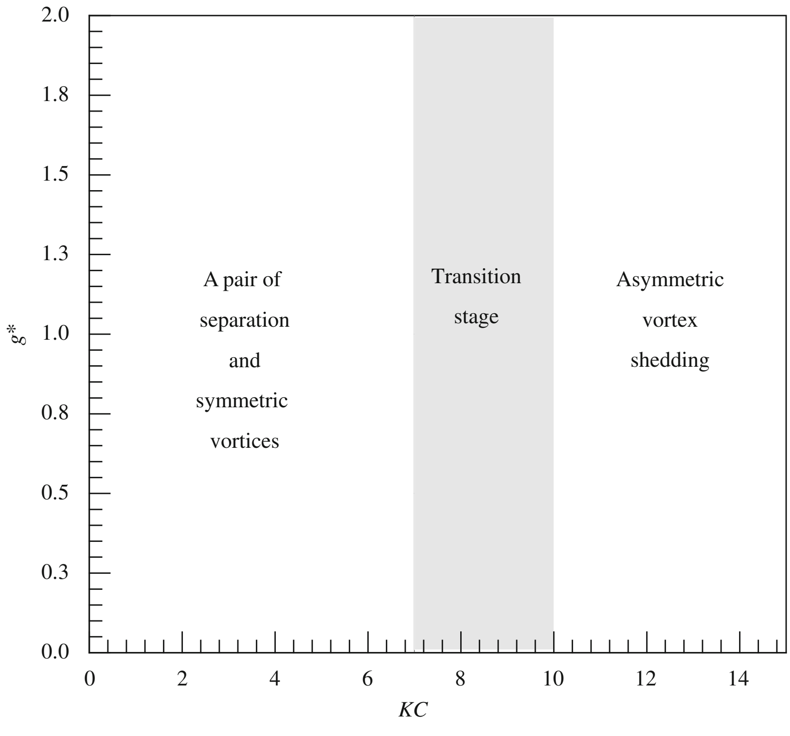

Fig. 13. Formation of vortices in connection with g* and KC.

3.3. Spectral analysis of the resultant force

Time histories of C_F for all the cases studied are analyzed using a fast Fourier transform (FFT) technique. Fig. 11 shows the power spectrum of C_F at various KC. The single harmonic at KC = 1 indicates that the behavior of C_F is periodic. As KC increases, sub-harmonics become excited, as shown in Fig. 11(b) and (c). The second sub-harmonic is twice the fundamental harmonic. Subsequently, more and more sub-harmonics are excited at increasing KC values.

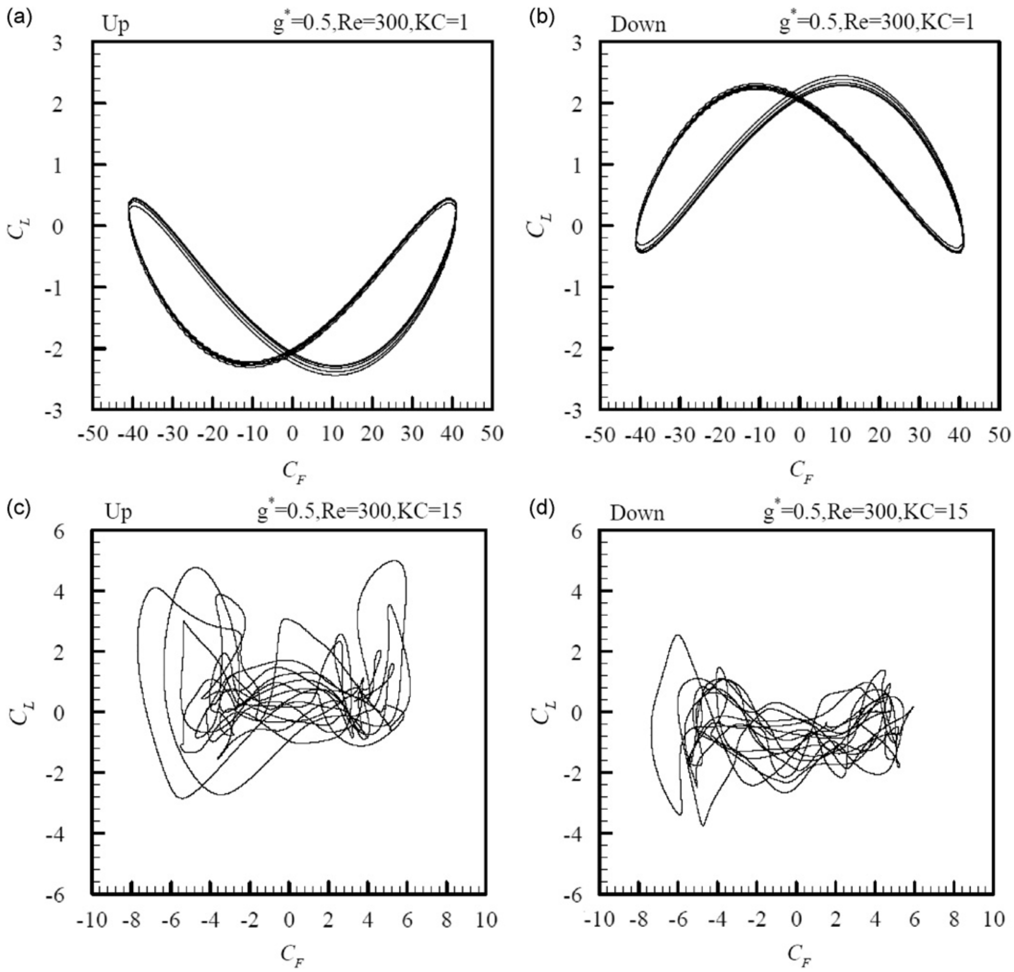

Fig. 14. Phase diagrams of C_F versus C_L. Re = 300 and $g^* = 0.5$.

Nonetheless, the fundamental harmonic still dominates C_F. When KC is increased to 15, the sub-harmonics are enhanced and therefore the behavior of C_F becomes more irregular, as shown in Fig. 11(c).

Influences of Re, KC, and g^* on time-averaged C_F are also investigated in this study. It is found that Re does not affect the time-averaged C_F. Fig. 12 shows the dependence of time-averaged C_F on g^* and KC. The amplitude of C_F, in Fig. 12, is inversely proportional to KC. As g^* decreases, C_F increases slightly. Variations of time-averaged C_F are fitted to three various curves denoted as lines and formulated as

$$C_F = 29.17\mathrm{KC}^{-7.87} \quad \text{for } g^* = 0.5, \tag{5}$$

$$C_F = 33.1\mathrm{KC}^{-8.41} \quad \text{for } g^* = 1, \tag{6}$$

$$C_F = 31.8\mathrm{KC}^{-8.61} \quad \text{for } g^* = 2. \tag{7}$$

Fig. 13 summarizes the vortex formation related to KC and g^*. Symmetric vortices form at KC = 7 for all the g^* values considered in this study, and asymmetric vortices form when KC > 10. The nonlinear phenomenon is shown in the phase diagram (Fig. 14) of C_F versus C_L for KC = 1 and 15, Re = 300, and $g^* = 0.5$. The results are shown for the upstream cylinder as well as the downstream cylinder. Perturbation does not occur at KC = 1, and the flow has periodic behavior, shown in Fig. 14(a) and (b). The pair of symmetric vortices is strongly coupled to each other. However, at large KC values such as KC = 15, perturbation causes a nonlinear chaotic state, shown in Fig. 14(c) and (d). The vortex

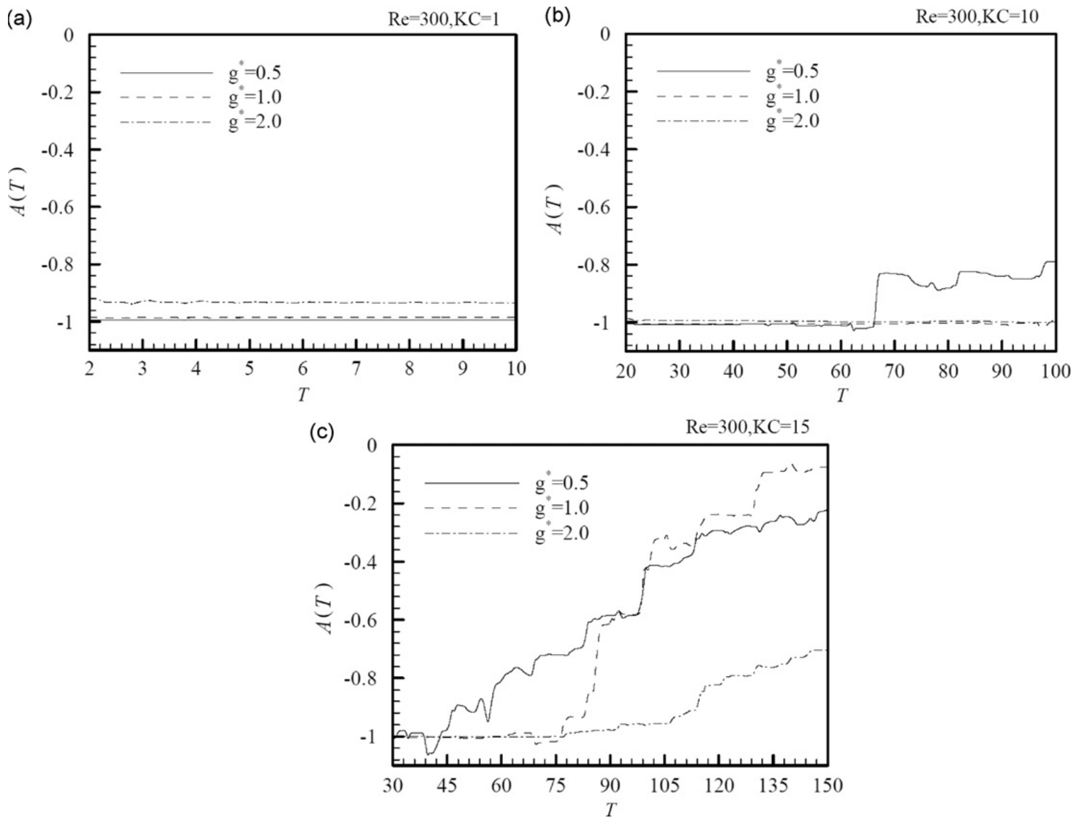

Fig. 15. Time histories of autocorrelation function $A(T)$ at Re = 300 and KC = 1, 10, and 15.

systems do not follow the same path as in Fig. 14(a) and (b). In order to determine the level of the relationship between vortex systems around upstream and downstream cylinders, the autocorrelation function $A(T)$ has been evaluated. Consider time histories of two functions of time $V_1(t)$ and $V_2(t)$. The autocorrelation $A(T)$ for these two functions $V_1(t)$ and $V_2(t)$ can be determined by the formula

$$A(T) = \frac{\overline{V_1 V_2}}{\overline{V_1^2}}, \tag{8}$$

where

$$\overline{V_1 V_2} = \lim_{T_f \to \infty} \frac{1}{T_f - T_i} \int_{T_i}^{T_f} V_1(t) V_2(t)\,\mathrm{d}t, \tag{9}$$

in which T_i and T_f refer to the initial time and final time, respectively. Provided V_1 is the same as V_2, $A(T) = 1$, corresponding to an in-phase state. Moreover, $A(T)$ becomes -1 when V_1 and V_2 are equal in magnitude but of opposite signs. Hence, V_1 and V_2 are in anti-phase. If V_1 is completely unrelated to V_2, then $A(T)$ will be zero. In addition, $A(T)$ varies from -1 to 1 when V_1 is partially related to V_2. Thus, $A(T)$ can be used to examine the degree of interaction between the vortex systems that form around two cylinders. The lift coefficient C_L is used here to characterize the vortex systems around two cylinders, such that

$$A(T) = \frac{\overline{C_L^U C_L^D}}{\overline{C_L^{U2}}}, \tag{10}$$

where the superscripts U and L refer to upstream and downstream cylinders, respectively. Fig. 15 shows $A(T)$ for Re = 300 and various g^* and KC values. Fig. 15(a) shows the time history of $A(T)$ at KC = 1. $A(T)$ remains -1 for all gaps, although it is about -0.9 for $g^* = 2.0$. This suggests that the two vortex systems are in anti-phase, as shown in Fig. 15(a). When KC increases to 10, the vortex systems in the vicinity of the cylinders are in anti-phase ($A(T) = -1$)

when $g^* = 1$ or 2 and KC = 10 as seen in Fig. 15(b). However, if the gap is sufficiently small (e.g. $g^* = 0.5$), $A(T)$ is not -1 all the time. Thus, these vortex systems are not in anti-phase but are partially related. The gap flow also plays a vital role in altering the anti-phase state. When KC increases to 15, $A(T)$ is not always -1 at the gaps, as can be seen in Fig. 15(c). Decreasing the gap brings forward the onset of increasing $A(T)$. Also, $A(T)$ is higher at KC = 15 than at KC = 1 or 10, and so such vortex systems do not strongly depend on each other any more. A very weak relation exists between these vortex systems at high KC.

4. Conclusions

Numerical simulations of an oscillating flow interacting with a pair of side-by-side square cylinders have been performed. Re, KC, and gap between the cylinders (g^*) were systematically varied and their influence on the flow physics was investigated. Reynolds number has less effect on the flow patterns, whereas KC and g^* play key roles in vortex formation. Up to KC = 7, a pair of symmetric vortices develops. The vortices remain symmetric until KC = 10, above which the vortices become asymmetric. When g^* is increased, additional vortices form in the flow direction. Gap flow has a major effect on vortex formation. In-line and lift coefficients have been determined, and a correlation obtained between C_F and KC. An FFT analysis of the time history of C_F indicates that the fundamental harmonic dominates the flow. Additional sub-harmonics are identified when KC is increased. The periodic solution turns chaotic in vortex systems in the vicinity of cylinders at increasing KC. The chaotic state occurs earlier for smaller cylinder gap ratio. From an analysis of the autocorrelation function $A(T)$ it appears that the vortex systems around two cylinders are strongly interdependent and are in an anti-phase state at low KC ($A(T) = -1$). Nevertheless, $A(T)$ increases with increasing KC because the two vortex systems become less dependent on each other.

Acknowledgements

The authors would like to express their gratitude for the support by National Science Council Taiwan (Project no. NSC 96-2212-E-011-098-MY3).

References

Bearman, P.W., Graham, J.M.R., Obasaju, E.D., Drossopulos, G.M., 1984. The influence of corner radius on the forces experienced by cylindrical bluff bodies in oscillatory flow. Applied Ocean Research 6, 83–89.

Bhattacharyya, S., Maiti, D.K., 2004. Shear flow past a square cylinder near a wall. International Journal of Engineering Science 42, 2119–2134.

Chern, M.J., Lu, Y.J., Jhang, S.J., Cheng, I.C., 2007. Interaction of oscillatory flows with a square cylinder. Journal of Mechanics 23, 245–250.

Davis, R.W., Moore, E.F., Purtell, L.P., 1984. A numerical–experimental study of confined flow around rectangular cylinders. Physics of Fluids 27, 46–59.

Franke, R., Rodi, W., Schonung, B., 1990. Numerical calculation of laminar vortex-shedding flow past cylinders. Journal of Wind Engineering and Industrial Aerodynamics 35, 237–257.

Honji, H., 1981. Streaked flow around an oscillating circular cylinder. Journal of Fluid Mechanics 107, 509–520.

Leonard, B.P., 1979. A stable and accurate convective modeling procedure based on quadratic upstream interpolation. Computer Methods in Applied Mechanics and Engineering 19, 59–98.

Obasaju, E.D., Bearman, P.W., Graham, J.M.R., 1988. A study of forces, circulation and vortex patterns around a circular cylinder in oscillating flow. Journal of Fluid Mechanics 196, 467–494.

Okajima, A., Ueno, H., Sakai, H., 1992. Numerical simulation of flow laminar and turbulent flows around rectangular cylinders. International Journal for Numerical Methods in Fluids 15, 999–1012.

Peng, Y.F., 2004. On the bi-stabilities of vortex shedding flows behind a pair of square solids. Journal of the Chinese Institute of Engineers 27, 385–393.

Saha, A.K., Muralidhar, K., Biswas, G., 2000. Transition and chaos in two-dimensional flow past a square cylinder. Journal of Engineering Mechanics 126, 523–532.

Sarpkaya, T., 1986. Force on a circular cylinder in viscous oscillating flow at low Keulegan–Carpenter numbers. Journal of Fluid Mechanics 165, 61–71.

Sumer, B.M., Fredsoe, J., 1997. Hydrodynamics Around Cylindrical Structures. World Scientific Publish Co., Singapore.

Testik, F.Y., Voropayev, S.I., Fernando, H.J.S., 2005. Flow around a short horizontal bottom cylinder under steady and oscillatory flows. Physics of Fluids 17, article no. 047103.

Williamson, C.H.K., 1985. Sinusoidal flow relative to circular cylinders. Journal of Fluid Mechanics 155, 141–174.

Williamson, C.H.K., 1996. Vortex dynamics in the cylinder wake. Annual Review of Fluid Mechanics 28, 477–539.

Yang, S.J., Chang, T.R., Fu, W.S., 2005. Numerical simulation of flow structures around an oscillating rectangular cylinder in a channel flow. Computational Mechanics 35, 342–351.

Zdravkovich, M.M., 1997. Flow Around Circular Cylinders. Oxford University Press, New York.

Zheng, W., Dalton, C., 1999. Numerical prediction of force on rectangular cylinders in oscillating viscous flow. Journal of Fluids and Structures 13, 225–249.

Zhou, Y., So, R.M.C., Liu, M.H., Zhang, H.J., 2000. Complex turbulent wakes generated by two and three side-by-side cylinders. International Journal of Heat and Fluid Flow 21, 125–133.